PAPER

An experimental study of an airfoil with a bio-inspired leading edge device at high angles of attack

To cite this article: Boris A Mandadzhiev *et al* 2017 *Smart Mater. Struct.* **26** 094008

IOP Publishing Smart Materials and Structures
Smart Mater. Struct. 26 (2017) 094008 (18pp) https://doi.org/10.1088/1361-665X/aa7dcd

An experimental study of an airfoil with a bio-inspired leading edge device at high angles of attack

Boris A Mandadzhiev, Michael K Lynch, Leonardo P Chamorro and Aimy A Wissa

University of Illinois at Urbana-Champaign, 1206 W. Green St., Urbana, IL 61801, United States of America

E-mail: awissa@illinois.edu

Received 1 February 2017, revised 15 June 2017
Accepted for publication 5 July 2017
Published 17 August 2017

Abstract

Robust and predictable aerodynamic performance of unmanned aerial vehicles at the limits of their design envelope is critical for safety and mission adaptability. Deployable aerodynamic surfaces from the wing leading or trailing edges are often used to extend the aerodynamic envelope (e.g. slats and flaps). Birds have also evolved feathers at the leading edge (LE) of their wings, known as the alula, which enables them to perform high angles of attack maneuvers. In this study, a series of wind tunnel experiments are performed to quantify the effect of various deployment parameters of an alula-like LE device on the aerodynamic performance of a cambered airfoil (S1223) at stall and post stall conditions. The alula relative angle of attack, measured from the mean chord of the airfoil, is varied to modulate tip-vortex strength, while the alula deflection angle is varied to modulate the distance between the tip vortex and the wing surface. Integrated lift force measurements were collected at various alula-inspired device configurations. The effect of the alula-inspired device on the boundary layer velocity profile and turbulence intensity were investigated through hot-wire anemometer measurements. Results show that as alula deflection angle increases, the lift coefficient also increase especially at lower alula relative angles of attack. Moreover, at post stall wing angles of attack, the wake velocity deficit is reduced in the presence of alula device, confirming the mitigation of the wing adverse pressure gradient. The results are in strong agreement with measurements taken on bird wings showing delayed flow reversal and extended range of operational angles of attack. An engineered alula-inspired device has the potential to improve mission adaptability in small unmanned air vehicles during low Reynolds number flight.

Keywords: alula, bioinspired adaptive structures, stall mitigation, wind tunnel test

(Some figures may appear in colour only in the online journal)

1. Introduction

Life has been evolving for millions of years, adapting to the environment and specializing in ecological niches. Bird wings evolved feather structures at the leading edge (LE), and some have a small wing-like structure, known as the alula (figure 1). Located between the hand wing and the arm wing, the alula is a digit bone controlled by several muscles and has 2–6 remiges, which are small versions of the primary flight feathers (figure 1) [1]. The alula is an aerodynamic device utilized by birds to increase their flight capabilities. Unlike fixed wing aerial vehicles, birds use and adapt their entire bodies to achieve efficient performance for multiple flight conditions. For example, take off and landing, maneuvering, or catching prey require unique aerodynamic capabilities. When landing, for instance, the bird enters a controlled descent, continuously reducing its speed. However, since the lift generated by the bird's wings has to equal its weight, the

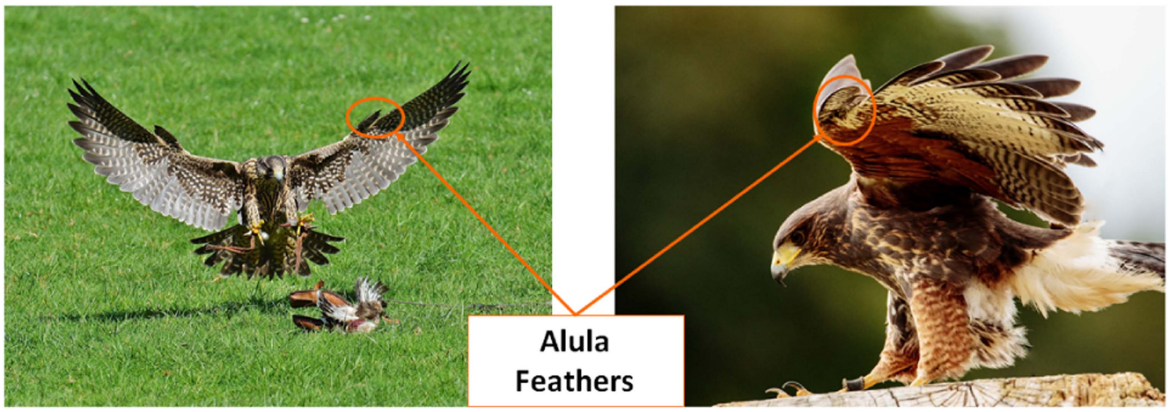

Figure 1. (Left) a falcon (photo by Alexas_Fotos/pixabay) and (right) a yellow-billed kite (photo by Kdsphotos/pixabay) in perching maneuvers with the alula wings deployed and discernible.

wings' angle of attack (AoA) has to be increased. Immediately before the end of the maneuver, the AoA exceeds the stall angle and the wing loses its ability to generate lift [2]. For such a maneuver to be executed in a controlled manner, a stall prevention device such as the alula is essential. A detailed explanation of the mechanism behind flow separation and stall can be found in [3].

There are two predominant effects of the alula structure on the aerodynamics of a wing in post stall conditions. One is the slat effect, which reduces the boundary layer (BL) velocity at the LE and the other is the alula tip vortex, which injects momentum into the BL. Both effects mitigate flow separation. When deployed, the alula deflects from the wing surface creating a narrow opening between the upper surface of the wing LE and the lower surface of the alula wing. In this manner the alula is similar to a LE slotted flap of fixed wing aircraft. Slots work by reducing the adverse pressure gradient over the LE of the wing, thus delaying flow separation at high angles of attack [4, 5]. Slots have been shown to increase the maximum lift coefficient of a wing by 37% and delay stall by 24° [5–7]. As described by Abbot and Doenhoff [5], a good BL control device can delay separation of both LE laminar flow as well as aft turbulent flow. In a series of studies, Weick *et al* [6–8] examined the performance of wings with LE slats in various configurations. In their studies, the slat airfoil shape, size, position and orientation were used as input parameters against which lift (C_l), drg (C_d) and pitching moment (C_m) were evaluated. Performance parameters showed sensitivity to all variable parameters tested but ubiquitously increased the maximum lift coefficient (C_{lmax}) and the aerodynamic efficiency ratio L/D. In addition to the slat effect, the alula behaves as a vortex generator (VG), because of the trailing vortex system formed at its tip. Basically, a set of counter rotating tip vortices, one on each wing, re-energizes the wing BL at high angles of attack, as described by Lee *et al* [9]. This combination of unique functions allows for increased lift at higher angles of attack, resulting in low stall speeds, high maneuverability, and better flight control.

To the best of the authors knowledge, no computational or numerical studies on an alula-like LE device exist. Due to the complexity involved in the aerodynamics of stalled airfoils, simulation-based studies are primarily focused on evaluating the fidelity of the numerical scheme and do not provide details on the performance of LE devices. Genc *et al* [10] evaluated, experimentally and numerically, the effect of a multi-element airfoil with NACA 22 LE slats and found that the LE slat significantly extended the stall angle to 20°. Shyy *et al* [11] evaluated the effect of Reynolds number (*Re*) on the leading edge vortex (LEV) and spanwise flow structures. When compared to the alula, LE slots are extensible features that span the full wing span section and as such do not utilize the trailing tip vortex system for separation control. Experimental and numerical investigations of both flapping and fixed wing leading edge VGs exist. For instance, similar to the alula device, in its function as a VG, the dogtooth feature on some transonic aircraft is used for separation control. At high AoA the dogtooth discontinuity reduce the outboard boundary-layer flow and delay tip stall [12–14]. Fixed, solid-VGs are simple, rugged and low cost but lack active flow control capabilities and they add parasitic drag in flow situations where stall mitigation is not required. LE serrations on flat plates at low Reynolds numbers [15] have been found to improve stall angle performance, but with a drag and lift penalties. Direct numerical simulation studies of passive VG flow separation control on NACA0102 airfoil [16], show a reduction in the size of the separation zone by more than 80%. Thus, stall mitigation and flow separation control via the use of LE devices has shown promising results. However, alula-like lifting surfaces that combine the functionality of LE slots and VGs have not been analyzed either numerically or experimentally.

This paper analyzes the performance of an airfoil equipped with a leading edge alula device (LEAD). The LEAD is designed as a lifting surface, able to generate lift and drag forces. In favorable local flow conditions and having an airfoil cross sectional shape, the LEAD generates circulation and an associated tip vortex system, as shown in figure 2. The formet tip vortex expands downstream and interacts with the wing upper surface BL (figure 2(a)). The plane of the generated downwash follows that of the alula device chord line.

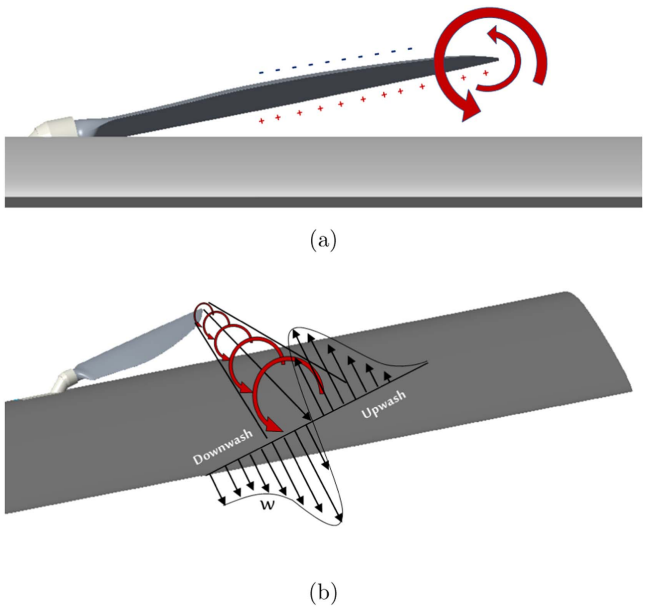

Figure 2. (a) Rear view of the alula counter-clockwise tip vortex as it expands and interacts with the wing upper surface boundary layer on the right wing. (b) The alula wing tip trailing vortex formation and associated downwash induced by the circulation expands and propagates in the streamwise direction. Downwash plane is angled to the wing chord line due to the alula deflection angle, γ.

As shown in figure 2(b), the tip vortex and downwash system impinges the wing BL injecting momentum extracted from the freestream and adding a spanwise velocity component to the wing BL, increasing its the ability to overcome the adverse pressure gradient at high angles of attack.

The goal of this work is to quantify the effect of the LEAD on lift, separation control and stall performance of a low *Re* high-lift airfoil at near and post stall regimes. The focus of this experimental study is to understand the effect of LEAD geometric parameters, such as the relative AoA (β) and tip deflection angle (γ) on lift performance, stall and separation behavior, airfoil wake structure, and BL velocity profiles.

A summary of previous work on bird wings with a detailed analysis of the alula function is given in the background section (section 2). Wind tunnel experimental setup, wing and alula airfoil selection and test schedules are described in section 3. In section 4, the results from force and hot-wire measurements are presented and their physical relevance is discussed. Section 4 also provides insight in the ability of the alula to influence the flow structure over the tested airfoil. Conclusion are presented in section 5 and suggestions on ways to expand this work can be found in section 6.

2. Background

The majority of the literature focusing on the alula is published by the biology community, where studies were conducted on wings of live or dead birds. An artificial LEAD was constructed by Meseguer *et al* [17] to study the effect of an alula-inspired device on lift production. Improvements in lift forces up to 20% are reported. Work published in the literature either focuses on the morphology of the alula or on understanding the aerodynamic effects. Results, from the biological community, show an increase in lift performance, stall mitigation and separation control due to the presence of the alula [9, 17–19]

On the morphological side, Alvarez *et al* [20], Crowford and Greenwalt [21], Savile [22] and Norberg [23] have studied the flight of a number bird species. Norberg discusses bird morphological flight parameters such as mass, length and area [23]. Important functional relationships between alula size, alula position, wing aspect ratio ($\mathcal{AR}$), and wing loading (W) were reported in references [20] and [22]. Alula span is shown to diminish with increasing wing aspect ratio, suggesting that only low $\mathcal{AR}$, high-lift wings require the extended alula surface. For example, birds that have moderate aspect ratio wings and that are required to produce high lift at slow flight speeds (e.g. *Owls, Storks*) almost always have a pronounced alula. These birds are efficient at low speeds and static soaring over land. This is also confirmed by the fact that the alula span increases with higher wing loading, especially in soaring bird species, where the demand for high lift is the highest [20]. Additionaly, more distal alula root spanwise locations are linked to high-lift wings, with thicker cross sectional airfoils, since they can sustain higher wing loading at the wing tips.

On the aerodynamic side, a few studies have been conducted to explain the function of the alula and its aerodynamic effects in birds [9, 18, 20, 24]. These studies used a combination of particle image velocimetry (PIV), lift-drag measurements and other methods to create quantitative descriptions and wing performance data. Test results by Lee *et al* show that when the alula is deployed, the wing of the adult male magpies generates ∼1%–12% more lift and delayed stall by ∼5°–10° [9].

Austin and Anderson [18] tested the wings of Wood Ducks, Black Scoters and Lesser Scaups at flow speeds of 7–20 ms^{-1} at AoA of −10° to 35°. They found that in all three tested bird species, the alula deflects at a specific velocity and AoA. Figure 3 shows that the alula deflection envelope increases in relation to AoA and flow velocity. An interesting observation is that the alula deflects at certain minimum conditions but then closes at a maximum AoA and velocity combination. The data markers in figure 3 denote the flight condition where the alula deflection was at a maximum. Digital PIV results indicate that the flow behind the wing with the alula deployed is faster and always non-reversed [18]. The authors suggest that the effect of the alula may be most pronounced in its ability to reduce stall risk rather than to serve as a lift enhancing device.

Lee *et al* concluded that, when deployed, the alula remiges create a counter-clockwise streamwise vortex moving downstream (figure 3(b)) [9]. The shear layer thickness over the top surface of the wing is decreased by the faster streamwise flow from the downwash flow vector created by the alula tip vortices [9]. The thinner shear layer causes delayed flow separation over the top of the bird wings from the vicinity of the alula towards the wing tips. Furthermore, as

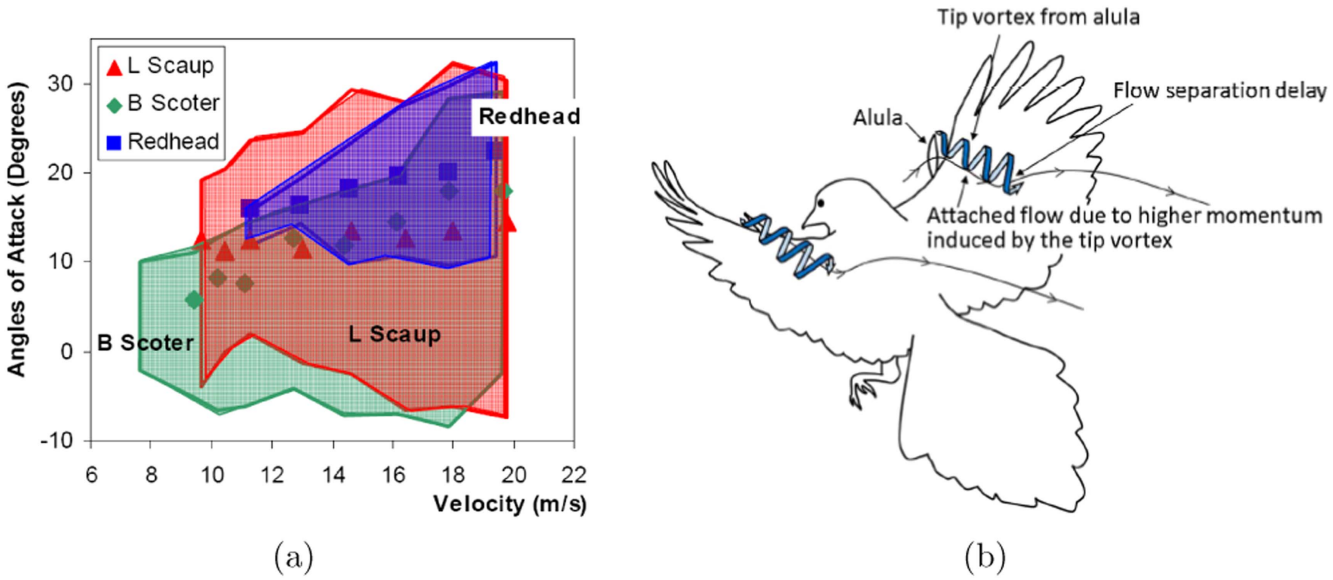

Figure 3. (a) Alula deployment envelope. Data points indicate AoA for maximum alula deflection. A trend can be observed in which the AoA at which maximum deflection occurs increases with higher velocities. Also, the minimum AoA for alula deflection decreases with increase in velocity. From Austin and Anderson [18]. (b) Counter-clockwise tip vortex formation from alula tips. From Lee *et al* [9].

the main wing AoA increases, the alula tip distance from the wing LE increases. This mechanism prevents the wing from losing its circulation due to viscous dissipation near the LE surface [9]. The authors also measured the relative angle between alula and wing chord lines to be $-29°$, suggesting that the alula does not generate lift at low AoA of the main wing [9]. Only at extreme wing AoA, the alula relative AoA to the freestream is sufficient to generate high strength tip vortex, imparting sufficient momentum on the suction side of the wing [9]. Furthermore, the counter-clockwise rotation of the stream-wise tip vortex induces spanwise velocity over the wing in the distal direction. In figure 4, the BL velocity profile with the alula deployed shows a delayed flow reversal in comparison to the clean wing. This suppresses the flow separation further and is more pronounced in the regions outside of the alula wing tips [9].

In summary, most of the work in the literature on the topic of LE devices for lift enhancements is either published by biologists or engineers. On the biology side, researchers have compared the alula morphological parameters of different birds and how these parameters vary according to the birds flight speed, habitat and overall size. Biologists have also measured and modeled the BL profile over a birds wing with its alula intact or removed. On the engineering sides, researchers have studied other lift enhancement devices such as slots and fixed VGs. This paper discusses a LEAD that combines the functionality of LE slots and VGs. This work adapts a biological device and tests it on an engineering system where any geometric or structural parameter can be varied and the effect of this variation can be studied. In this paper, we will primarily focus on two parameters namely, the alula deflection angle and the alula relative AoA and we will investigate and measure the effect of varying these parameters on lift production, BL profile, and turbulence characteristics.

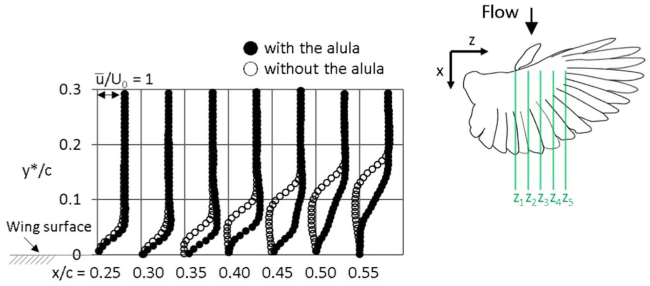

Figure 4. Wing upper surface boundary layer velocity profiles at location Z_2 location, with alula—solid circles, without alula—hollow circles. Wing AoA is 24°. Vertical axis is speed and is normalized to the mean freestream velocity of 3 m s^{-1}. Horizontal axis is normalized to the chord length of the wing and the data points run to the location where boundary layer flow reversal begins. From Lee *et al* [9].

The results presented provides a better understanding of the role of an alula-inspired device in low *Re* flight.

3. Experimental setup

3.1. Test setup and measurement techniques

A two-dimensional airfoil equipped with an alula device was tested in a closed section, open-loop, constant pressure wind tunnel. The wind tunnel has a cross section of 44 cm height and 90 cm width. The airfoil was placed near the entrance of the test section to ensure nearly uniform conditions along the cross section, where the flow is characterized by low turbulence levels (0.1%). The wing section spanned the total height of the wind tunnel to eliminate three-dimensional effects of the wing.

Based on the chord length, the test velocity range was selected to produce Reynolds numbers of $Re = 1.0 \times 10^5$

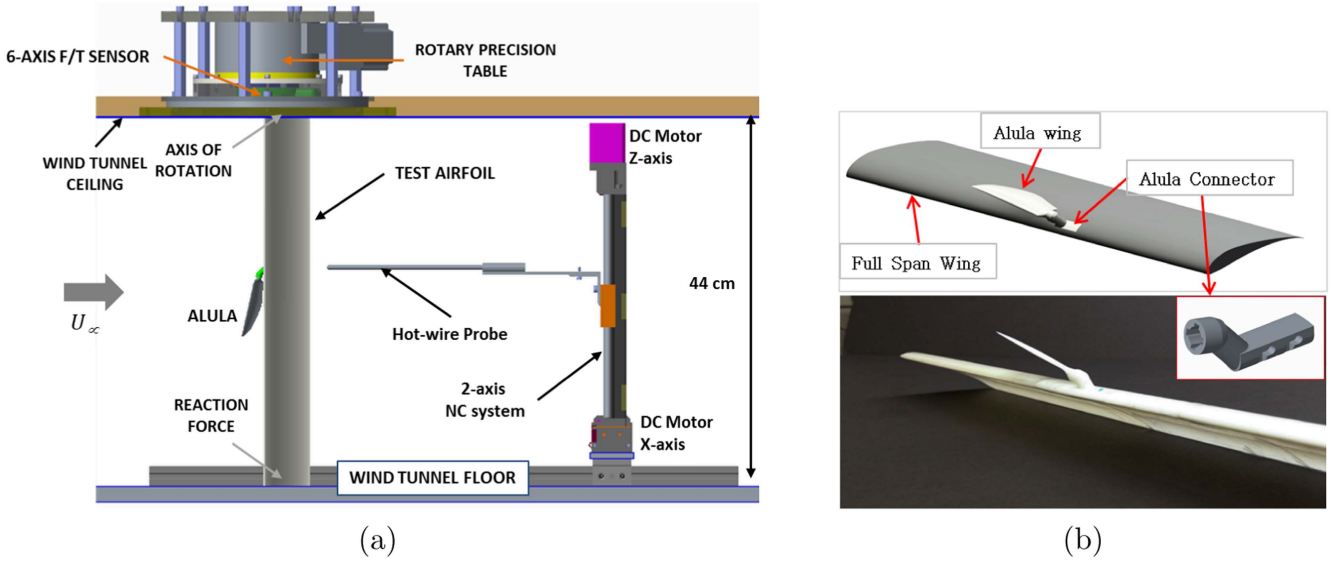

Figure 5. Detailed schematic of the experimental setup and alula device and wing system test specimen. (a) Hot-wire probe is located behind the TE and traverses along the span and out of the wing plan. (b) The alula device is attached through an adjustable connector to allow for β and γ adjustment.

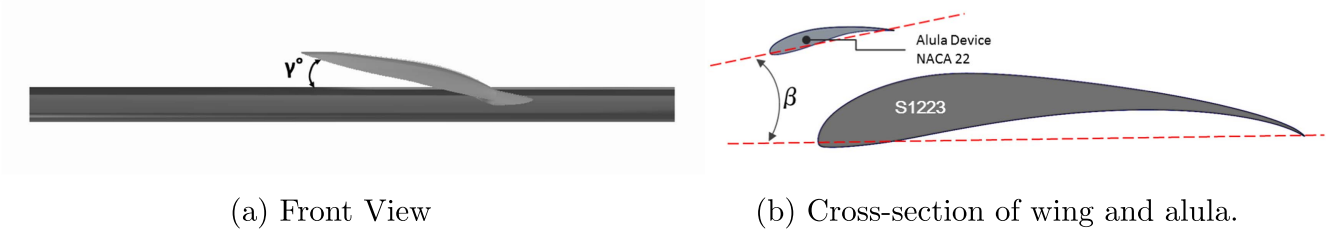

Figure 6. Schematic of the (a) front and (b) side views of the wing model equipped with an alula device showing the device's deflection angle, γ, and relative angle of attack, β.

and $Re = 1.35 \times 10^5$, which are representative of bird flight and most small UAVs' flight conditions. The parameters, which were varied during the test were the wind speed, wing AoA, alula deflection angle (β), and alula AoA (γ). The alula AoA was measured relative to the wing chord line. Figure 5 shows a schematic of the detailed experimental setup including the location of the force transducer and the downstream position of the hot-wire probe. Force measurement data was collected and and correlated to hot-wire BL measurements to better understand the aerodynamic effects of an alula device near and psot stall. The following subsections detail the measurements methods and uncertainties.

3.1.1. Force and velocity measurements and data acquisition. The effect of the alula-like device on the airfoil's over all lift was quantified using an ATI Industrial Automation 6-axis force and torque transducer. The force/torque transducer was used to sample lift, drag and pitch measurements and was attached to a stepper motor precision rotary table, which was affixed to the wind tunnel ceiling and used to set the airfoil AoA (see figure 5). The stepper motor was controlled from a computer through a control board and provided reliable angle positioning. The transducer has a high signal-to-noise ratio, a sensitivity of 1/160 N (0.006 25 N, and a saturation levels of 35 N of force per axis channel and 2.5 Nm torque per torque channel. Calibration was supplied by the manufacturer at 1% of the full measurement scale for each force axis. In order to avoid saturating the $+X$ and $+Y$ axis of the sensor due to aerodynamic forces, the airfoil section was supported by a reaction force at the floor of the test section. The airfoil was free to rotate around a pivot point at the quarter chord location. A gap smaller than 4 mm between the wing and wind tunnel wall was measured. Force and torque data were collected using a NI cDAQ-9133 Controller and NI 9205 analog input module. The velocity at the test location was measured using a standard laboratory pitot-static tube, a differential pressure sensor and NI 6009 data-acquisition unit. The probe was positioned 5 chord lengths upstream of the wing and alula test system. Pitot tube positioning technique assured flow alignment within $\pm 5°$ resulting in 1% uncertainty in measured flow velocity [26].

3.1.2. Hot-wire measurements. In order to characterize the effect of the alula on the wake velocity profile and turbulence intensity, a hot wire probe was placed behind the trailing edge (TE) of the airfoil at $x/c = 1.125$ (10 mm behind the TE), as shown in figure 5. The hot-wire probe used was a BL miniature wire probe (55p15) with a support sting (55h21). All hot-wire anemometry (HWA) measurements were

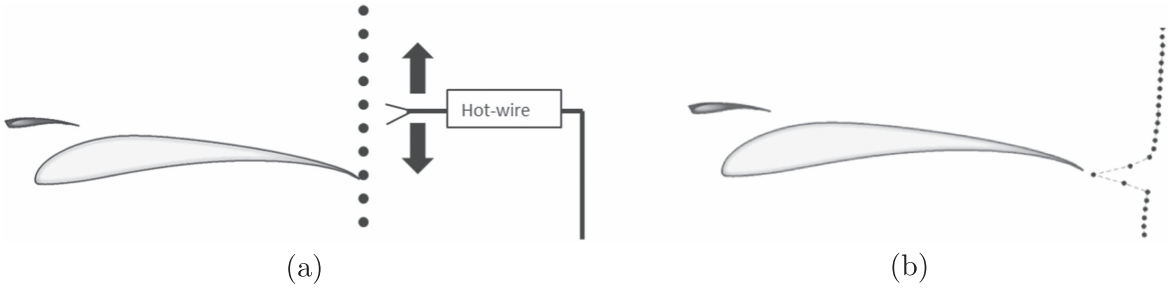

Figure 7. Hot-wire probe location is fixed for all tests at $x/c = 1.125$ and is translated through the BL of the airfoil. (a) Hot-wire probe stations across boundary layer at T.E., $x/c = 1.125$. (b) Sample results—velocity deficit overlayed on airfoil schematic.

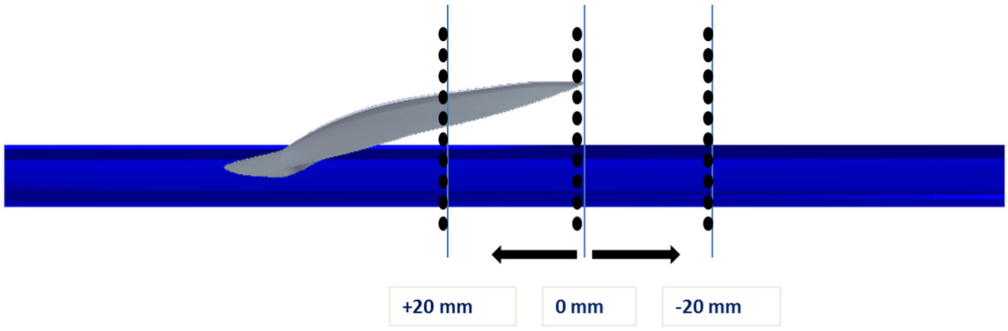

Figure 8. The hot-wire probe wire was translated int the span wise directions. Measurements were collected 20 mm inboard of the alula tip, at the alula tip, and 20 mm outboard of the alula tip. Note: figure not drawn to scale.

processed and stored with DANTEC StreamlinePro DAQ frame at a sampling frequency of 40 kHz, resulting in a frequency domain that contains the entire size range of flow features. The hot-wire probe was attached to a CNC precision table and traversed through the BL in discrete, pre-defined locations. At each sample location, 30 s elapsed before data recording was started, thus vibrations and flow unsteadiness due traversing were eliminated. A baseline test was conducted at each Reynolds number (Re) (i.e. $Re = 100\,000$ and $Re = 135\,000$) with the hot-wire positioned at mid-span (equidistant from wind tunnel walls) and translated through the BL, as shown in figure 7. A baseline test is defined as a test with no alula attached to the airfoil. For configurations with an alula device, the hot-wire probe was also translated through the BL. Data was also collected at three span-wise locations specifically, at −20, 0, and +20 mm from the alula wing tip (figure 8).

3.1.3. Total measurement system uncertainty. The uncertainties in the results were determined with the Kline–McClintock technique [25]. Force and torque measurements were subject to the highest level of measurement uncertainties due to the sensors and DAQ instrumentation used. The largest source of error is the ATI 6-axis force/torque sensor, especially at the lower wing incidence angles because generated lift values are small. The uncertainty of the force/torque sensor is reported by the manufacturer as a fraction to the sensor full measurement scale. Uncertainties in the AoA, flow velocity, air density, and DAQ signal analog input were also considered in estimating the aggregate error in measuring the lift coefficient, C_l. The total uncertainty in C_l measurements was calculated to be $<4\%$ in all test conditions.

3.1.4. Wake blockage effects. The closed section wind tunnel sidewalls restrain the natural curvature of the flow around an airfoil, causing the airfoil to behave as one with extra camber. Solid and wake blockage are effects on the flow field, which result from the presence of test section walls. Formulation for blockage and wake effects are summarized by Barlow *et al* [26] and the solid blockage increment is computed using equation (1).

$$\epsilon_{s_b} = K_1/C^{3/2}. \tag{1}$$

$K_1 = 0.000\,174\ \mathrm{m}^3$ is the volume of the tested wing section and $C = 0.4275\ \mathrm{m}^2$ is the wind tunnel test section cross sectional area (table 1), resulting in solid blockage effect of $\epsilon_{s_b} = 0.1\%$. Wake blockage effects were also considered, but due to the fact that the airfoil is a streamlined object, at relatively shallow incidence angles, the effect is negligible. Furthermore, since the trailing vortex system that impinges the BL is weak, downwash effect corrections were not considered [26]. Buoyancy effects were also not considered due to the absence of a longitudinal pressure gradient in the wind tunnel.

3.2. Wing and alula geometric parameters and experimental matrix

3.2.1. Wing and alula airfoil sections. The geometry of the tested wing section is based on previously published wing and alula shape parameters of different bird species [18, 20, 27, 28]. Table 1 compares the airfoil geometry tested in this paper to

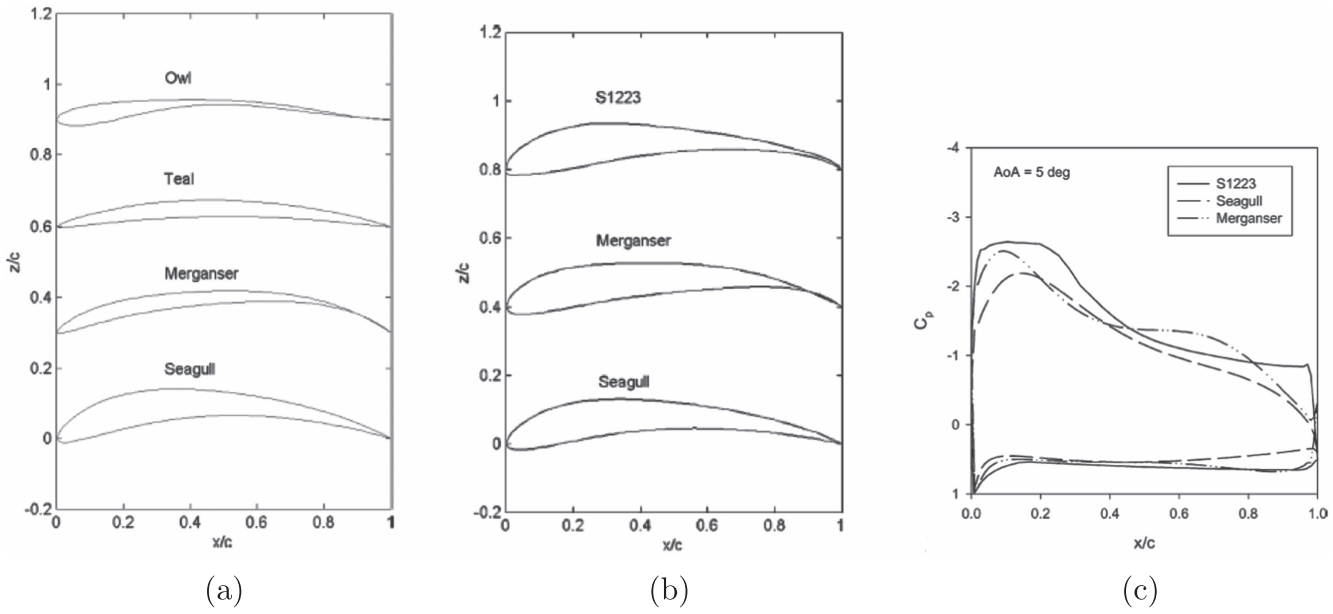

Figure 9. Wing airfoil section comparison between various bird species and a high-lift, low-Reynolds number airfoil, the S1223, by Selig *et al* [29–31]. (a) Laser scanned distal wing airfoil sections for Owl, Teal, Merganser and Seagull. (b) Comparison between highly cambered, high-lift airfoil S1223 to the Seagul and Merganser proximal wing sections. (c) Pressure coefficients at $\alpha = 5°$. On top and bottom airfoil surfaces are comparable.

Table 1. Wing morphological measurements of various bird species [18].

Bird specimen	Area $S(\text{cm}^2)$	Wing span b(cm)	Mean wing chord c(cm)	$\mathcal{AR}_{\text{wing}}$	Alula length b_A(cm)	Mean alula chord c_A(cm)	$\mathcal{AR}_{\text{alula}}$
Tested wing section	171.3	22.5	8.0	2.80	6.7	1.9	3.6
Black scoter	206.5	63.5	11.4	5.56	5.1	1.5	3.4
Lesser scaup	180.6	53.3	9.5	5.60	3.8	1.0	3.8
Redhead duck	240.0	61.0	11.1	5.49	5.1	1.5	3.4

other bird wing sections. Birds' wing section geometry were adapted from [29] where a three-dimensional laser scanner was used to measure wing surfaces non-intrusively. The choice for the test wing geometry stems from the combined wing planform characteristics shown in table 1 and the cross sectional airfoil studies shown in figure 9 [24, 29, 30]. As shown in figure 9(b), the S1223, camber line and thickness coordinates are similar to the ones of Seagulls and Merganser [29].

The S1223 airfoil is commonly used for high lift RC competition airplanes. It has maximum thickness of 12.1% at 19.8% chord and maximum camber of 8.1% at 49% chord. The span and chord lengths of the LEAD are 67.5 mm and 18.7 mm, respectively, with the span being 15% of the total wing span. The $\mathcal{AR}$ of the wing is based on a rectangular wing spanning the full wind tunnel height. The wing $\mathcal{AR}$ is reported despite the fact that the wing section spanned the whole wind tunnel to provide a dimensional similarity between the wing and the LEAD $\mathcal{AR}$. The LEAD wing has an elliptical planform and an NACA 22 airfoil cross section with a 12% maximum thickness at 24.2%c and 68% maximum camber at 54.2%c. This airfoil section is often used for LE devices in fixed wing applications because of its soft stall behavior and extended range of operational angles of attack.

3.2.2. Wing and alula test parameters and test matrices. The goal of this study is to analyze stall and deep stall behavior of the S1223 airfoil in the presence of a LEAD at low *Re* number. Thus, The three angles of attack tested were $\alpha = 4°$, $\alpha = 10°$, and $\alpha = 18°$ representing pre stall, stall and post a stall conditions, receptively. the two LEAD morphological parameters varied were the deflection angle (γ) and relative AoA (β). The highest deflection angle, $\gamma = 22°$, was extracted from several frontal pictures of perching maneuvers of owls and eagles. The lowest deflection angle possible was selected to be 4° due to physical interference between the LEAD and the wing upper surface. A mid-point angle of 13° was also tested to observe the effect of varying the wing deflection angle. The alula relative AoA was selected based on the wing AoA, α. The alula airfoil profile stalls at approximately 10°. The alula relative AoA (β) was selected such that, at the maximum wing AoA tested, the alula angle of incidence relative to the flow did not exceed 10° to avoid stall. Thus, the values of β tested ranged from $-10°$ to 10° in increments of 5°. Figure 6(a) shows a front

Table 2. Boundary layer (hot-wire) experimental test matrix. Alula deflection angle was fixed at $\gamma = 13°$ for all tests.

		$Re = 100\,000$				$Re = 135\,000$			
			$\beta°$				$\beta°$		
		Baseline	−10	0	10	Baseline	−10	0	10
$\alpha°$	4	X	X			X			
	10	X	X	X		X	X	X	X
	18	X	X	X	X	X	X	X	X

view the wing and alula setup, while figure 6(b) shows a cross sectional view and defines the alula relative AoA.

Force and torque data were collected at both *Re* numbers (i.e. $Re = 100\,000$ and $Re = 135\,000$) and at all wing angles of attack, alula deflection angles, and alula relative angles of attack. Due to the resource intensive nature of HWA testing, a smaller test matrix (table 2) was completed to investigate the effects of the alula morphological parameters on pre-stall, stall and post-stall wake profiles and turbulence levels. Baseline tests were conducted to establish reference BL profiles for comparison and to understand flow reversal and stall mechanisms close to the surface of the airfoil.

4. Results and discussion

This section discusses the effect of the LEAD on lift production and turbulence characteristics of the S1223 airfoil. Three AoA conditions, $\alpha = 4°$, $\alpha = 10°$ and $\alpha = 18°$ were tested in a systematic experimental approach at two wind tunnel freestream velocities corresponding to $Re = 1.0 \times 10^5$ and $Re = 1.35 \times 10^5$. In addition, three levels of alula deflection angles, $\gamma = 4°$, 13°, 22°, and five levels of alula relative AoA, $\beta = -10°$, −5°, 0°, 5°, 10° were considered to understand the effect of the alula morphological parameters on the aerodynamics. Results are divided into three main subsections. The first two subsections present the lift coefficient (C_l), wake velocity profile and turbulence intensity measurements for $Re = 1.0 \times 10^5$ and $Re = 1.35 \times 10^5$, respectively. The third subsection describes flow structures obtained through HWA measurements. HWA results, in the form of wake velocity profile and turbulence intensity levels, are used to explain the differences observed in the lift generated by various configurations at stall and post stall conditions.

4.1. Lift and wake profile for Re = 1.0 × 10^5

Figure 10 shows the lift coefficient at different alula tip deflection angles and relative AoA. At $Re = 1.0 \times 10^5$, the C_l–α curve for the S1223 has a sharp transition to stall conditions at $\alpha \approx 7°$ [32]. Figure 10(a) indicates that, prior to stall conditions (i.e. at $\alpha = 4°$), no alula configurations show an increase in C_l, suggesting that the alula is a device designed to deploy in post stall conditions. The response parameter, C_l, is sensitive to an increase in alula deflection angle, γ. There is strong correlation between increasing γ and positive change in C_l. At $\alpha = 18°$ and 4° (figure 10(c)), $\gamma = 22°$ shows the most lift improvements when compared to the other deflection angles. This is a result of the alula tip extending further into the wing's LE BL, which gives it access to the higher momentum freestream flow. This mechanism allows for more energy to be extracted and transferred to the wing BL through the alula tip trailing vortex. This correlation trend is only reversed at $\alpha = 10°$ and negative alula deflection angles, $\beta = -10°, -5°$ (figure 10(b)), when $\gamma = 4°$ produces the highest C_l improvement. This can be explained by the slat effect being the dominant aerodynamic phenomenon at negative alula angles, $\beta = -10°, -5°$ and low deflection angles. C_l is also sensitive to the alula relative AoA, β. Positive change in C_l is observed at lower alula angles, with maximum C_l achieved at the lowest alula AoA, namely $\beta = -10°$. The inverse relation between α and β is expected, since the alula local AoA must be below 10° (based on the onset of stall for the NACA 22 airfoil) for proper alula device operation.

Figures 11(a) and (b) show the wake profile and turbulence intensity measurements for the airofil with and without a LEAD at $\alpha = 10°$ and $Re = 1.0 \times 10^5$. Results are shown for $\gamma = 13°$ and $\beta = 0°$ and −10°. Reduction in wake deficit is only observed inboard of the alula tip, $z = +20$ mm, and resembles that of a slat effect by decreasing the size of the separation region significantly. Reduction in the wake deficit can be realted ot reduced drag and delayed separation. At $z = 0$ mm and $z = -20$ mm, there is no strong tip vortex effect at the wing surface, and the wake profile is unchanged or widened. The wake size can also be inferred from figure 11(b), which represents the flow turbulence intensity levels, I_n. An increase in turbulence levels is associated with the shear layer that exists between the high velocity free stream and the highly mixed, reversed flow wake. Figure 11(b) shows that there is a shift in the shear layer location and size with respect to the span-wise location. At the alula root ($z = +20$ mm), the wake region shear layer is observed to diminish at $y/c =$ 0.3, 0.35, and 0.42 for $\beta = 0°$, $\beta = -10°$ and the baseline configurations, respectively, which correlates to the wake velocity deficit reduction. In contrast, outboard of the alula tip ($z = -20$ mm), the order is reversed with respect to β. The increased distance of the shear layer beyond the alula for all β configurations can be explained by the higher physical location of the tip.

The S1223 airfoil at $Re = 1.0 \times 10^5$ and $\alpha = 18°$ is severe stall. At this AoA, $\beta = -10°$ shows improved

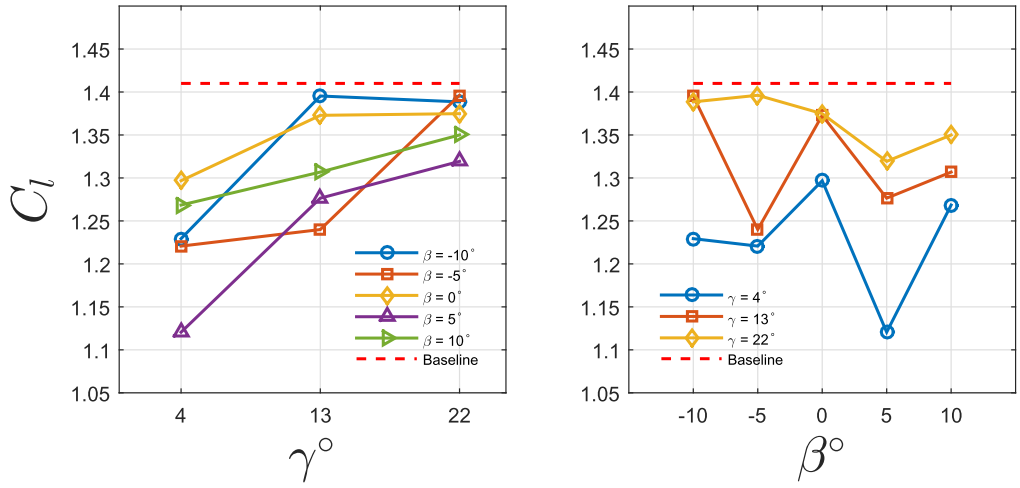

(a) $\alpha = 4^\circ$

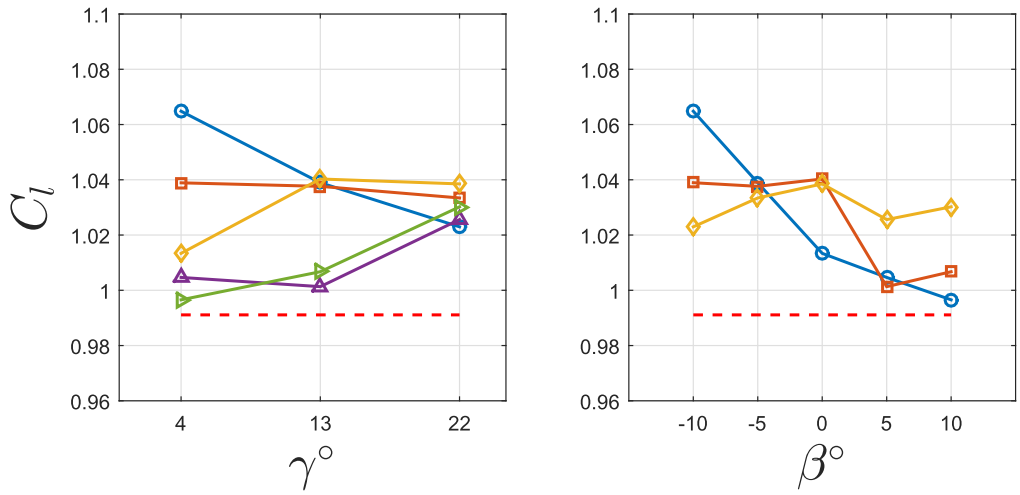

(b) $\alpha = 10^\circ$

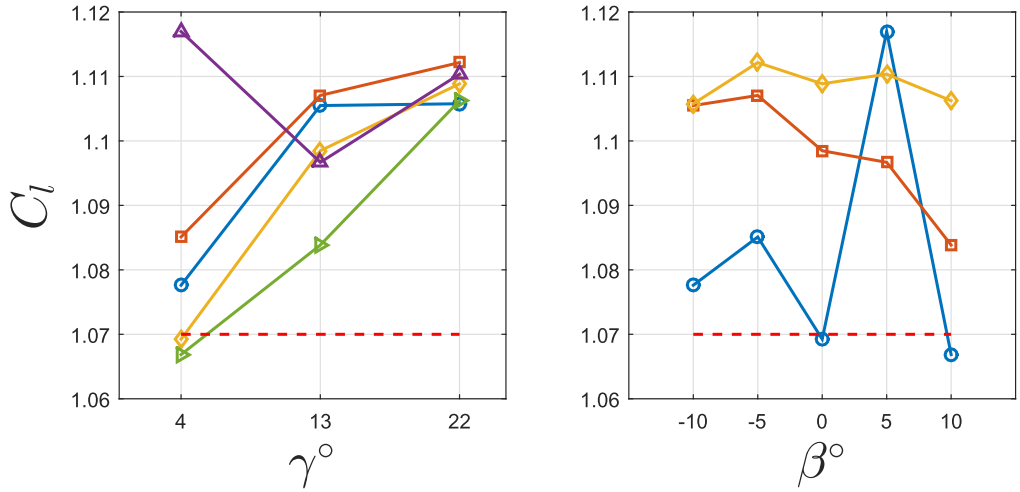

(c) $\alpha = 18^\circ$

Figure 10. Interaction plots between the lift coefficient, C_l and the alula parameters, β and γ at (a) $\alpha = 4^\circ$, (b) $\alpha = 10^\circ$, and (c) $\alpha = 18^\circ$ at $Re = 1.0 \times 10^5$. The doted horizontal line indicates the C_l value for the baseline configuration.

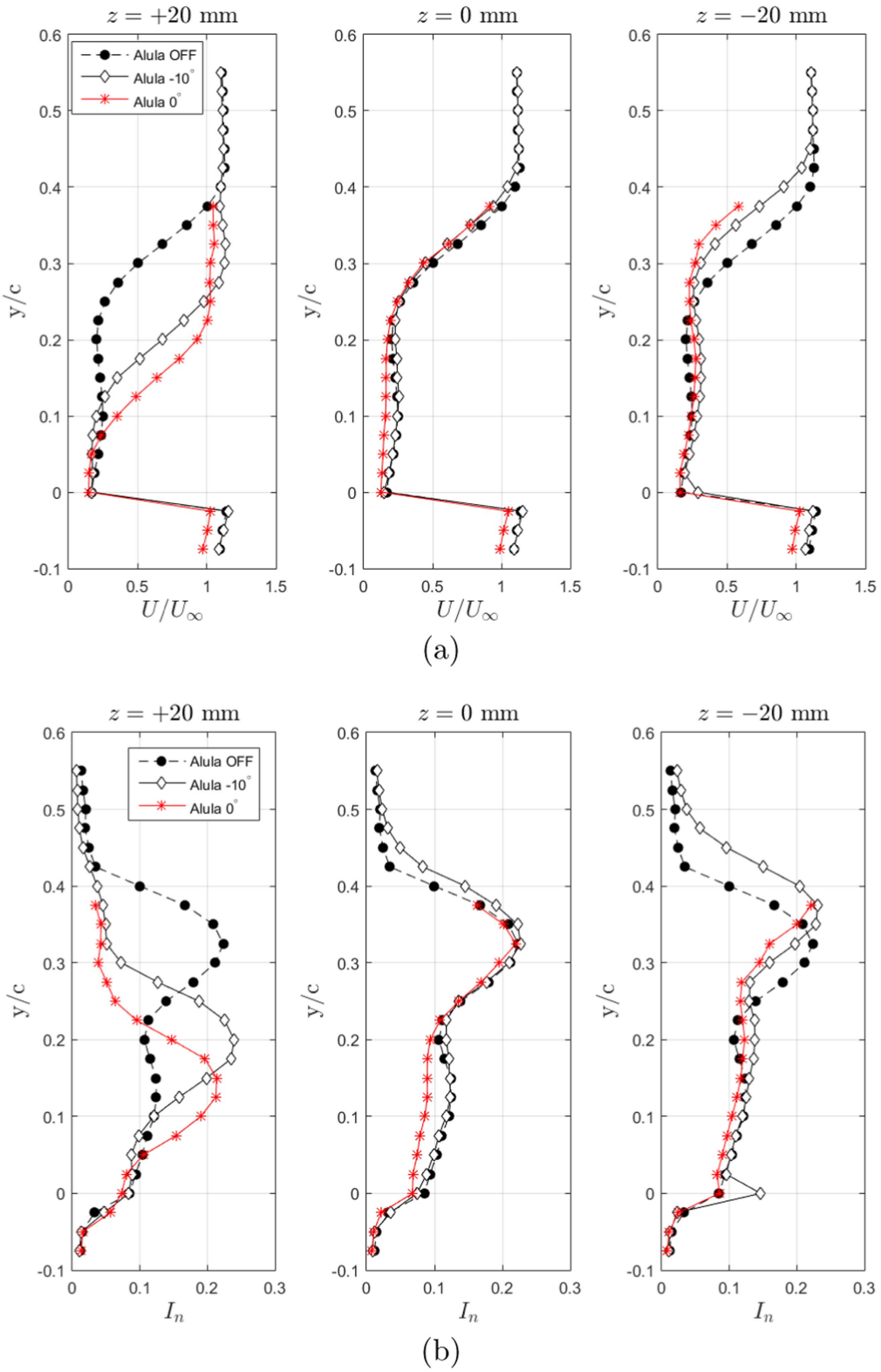

Figure 11. (a) Wake velocity profiles, U/U_∞ and (b) turbulence intensity levels, I_n for the airfoil with and without an alula-inspired device at $\alpha = 10°$, $\gamma = 13°$, and $Re = 1.0 \times 10^5$. The alula effect is primarily seen at the inboard section of the alula, $z = +20$ mm, with $\beta = 0°$ reducing the wake velocity deficit the most. Turbulence intensity levels follow similar trend with $\beta = 0°$ having the nearest to the wing surface shear layer.

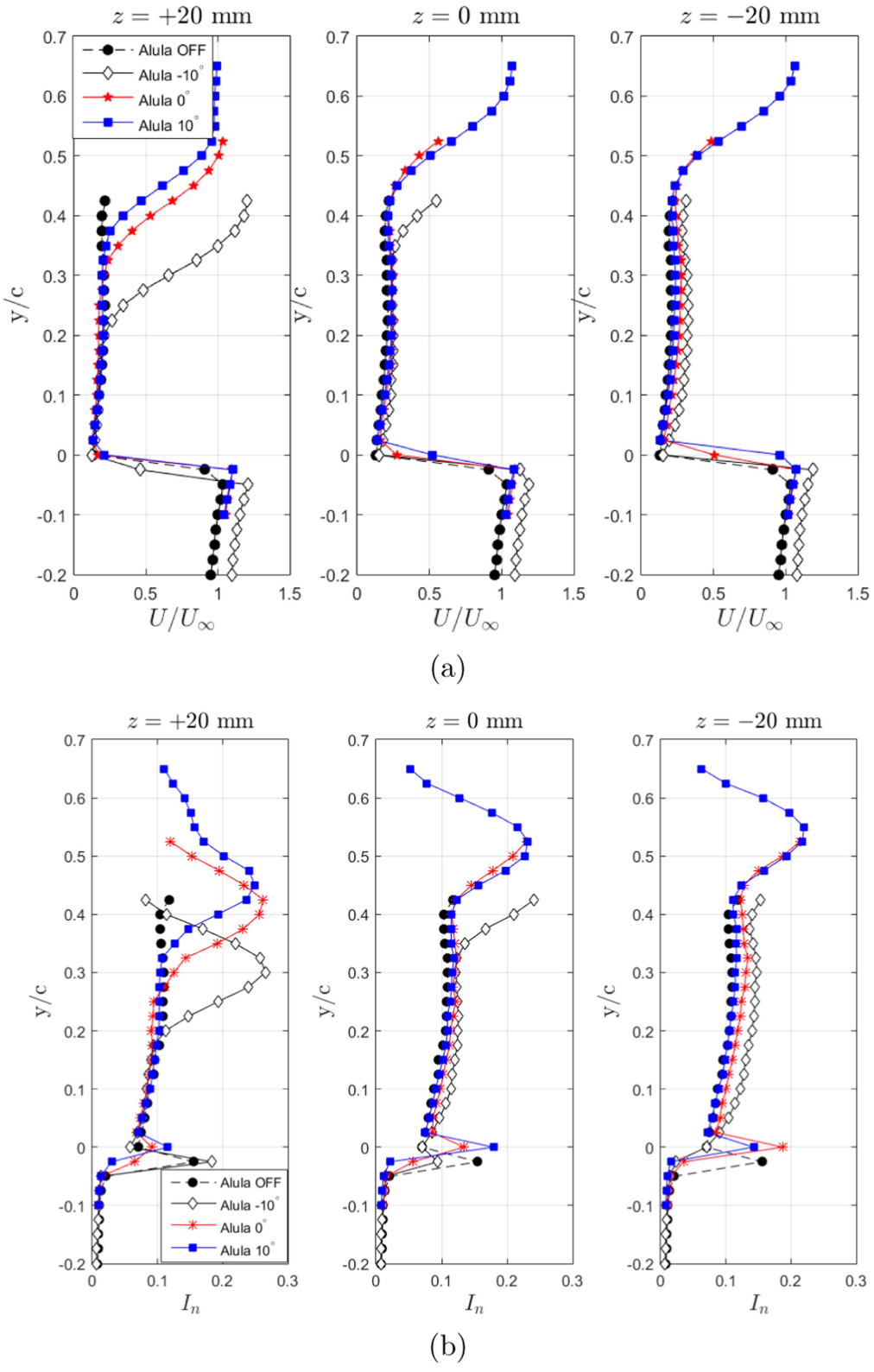

Figure 12. (a) Wake velocity profiles, U/U_∞ and (b) turbulence intensity levels, I_n for the airfoil with and without an alula-inspired device at $\alpha = 18°$, $\gamma = 13°$, and $Re = 1.0 \times 10^5$. The alula effect is primarily seen at the inboard section of the alula, $z = +20$ mm, with $\beta = -10°$ reducing the wake velocity deficit the most. Turbulence intensity levels follow similar trend with $\beta = -10°$ having the nearest to the wing surface, shear layer.

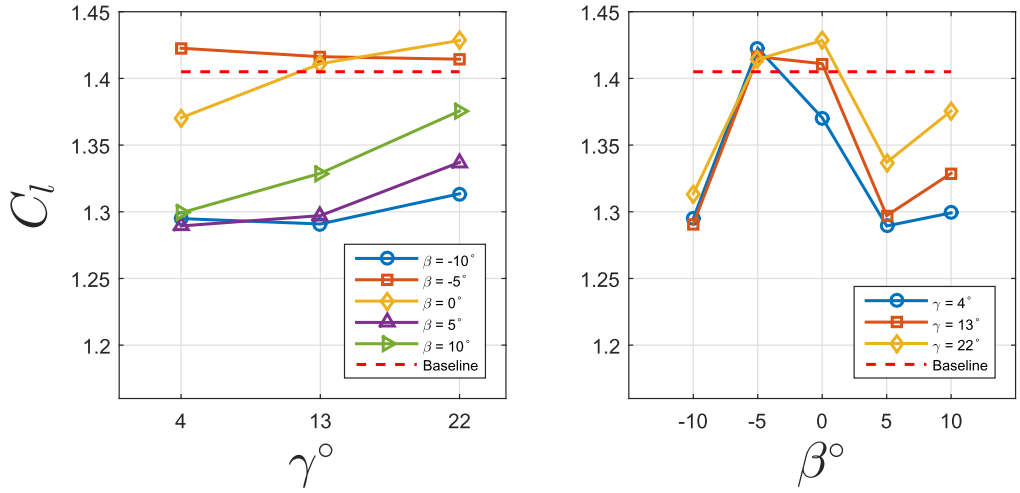

(a) $\alpha = 4^\circ$

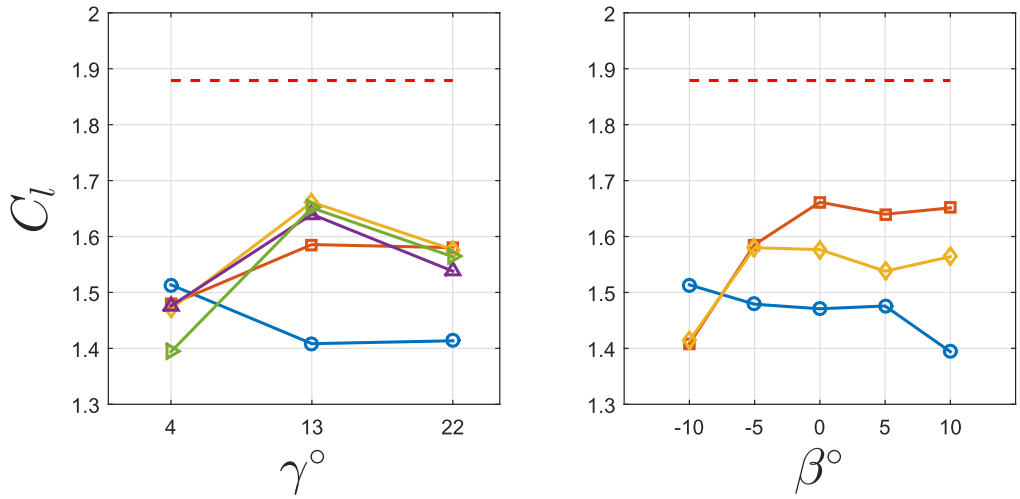

(b) $\alpha = 10^\circ$

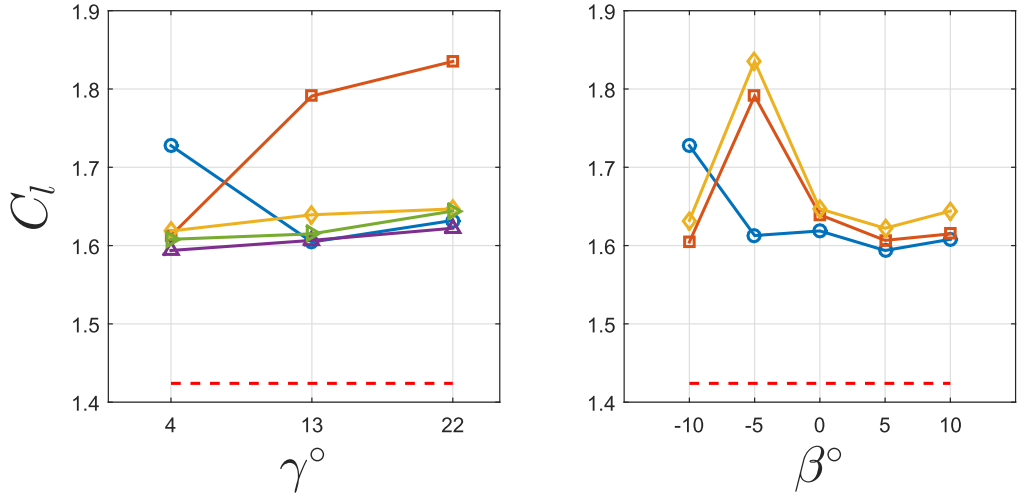

(c) $\alpha = 18^\circ$

Figure 13. Interaction plots between the lift coefficient, C_l and the alula parameters, β and γ at (a) $\alpha = 4^\circ$, (b) $\alpha = 10^\circ$, and (c) $\alpha = 18^\circ$ at $Re = 1.35 \times 10^5$. The doted horizontal line indicates the C_l value for the baseline configuration.

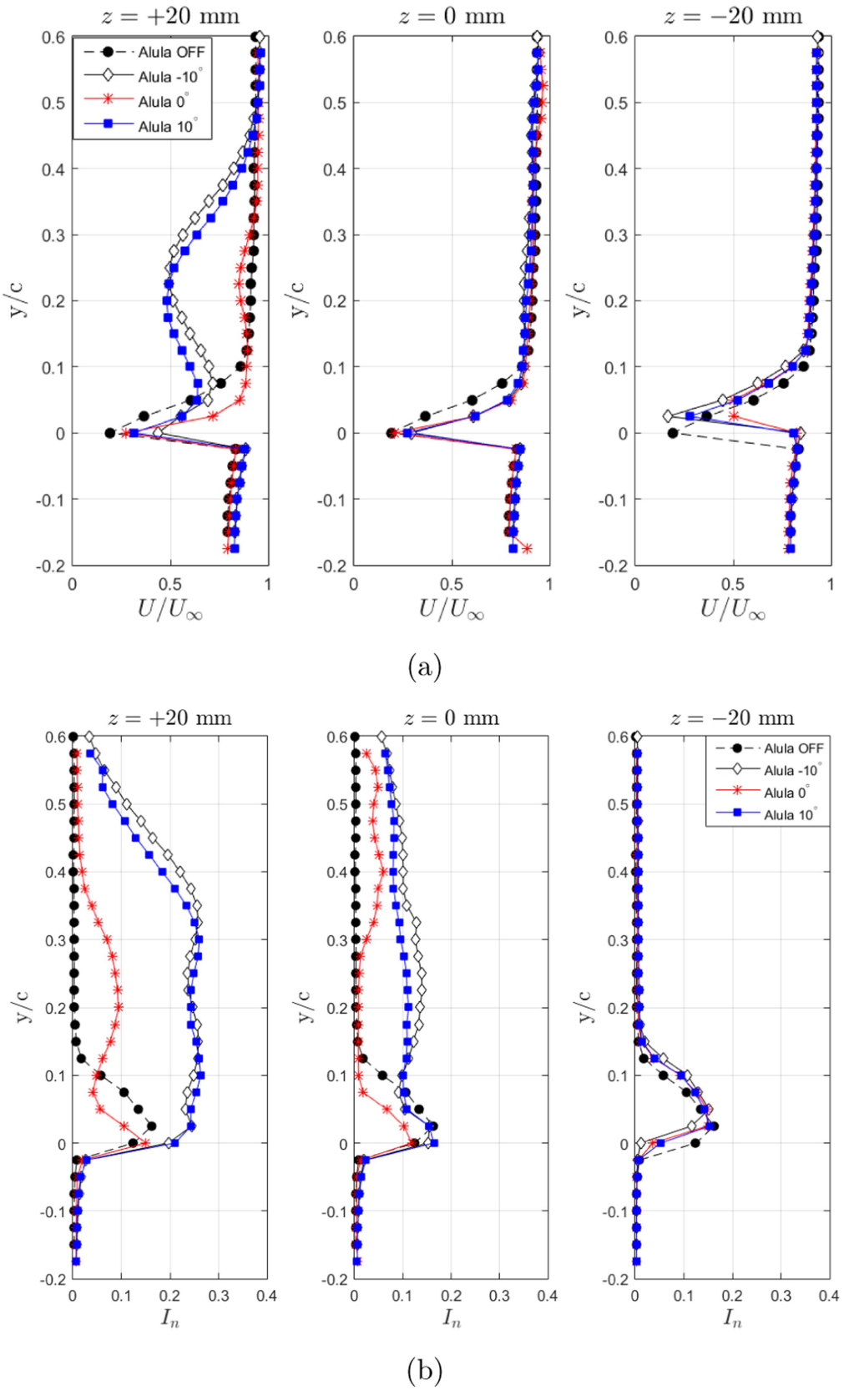

Figure 14. (a) Wake velocity profiles, U/U_∞ and (b) turbulence intensity levels, I_n for the airfoil with and without an alula-inspired device at $\alpha = 10°$, and $Re = 1.35 \times 10^5$. The alula effect is primarily seen at the inboard section of the alula, $z = +20$ mm, with $\beta = -10°$ reducing the velocity deficit the most. Turbulence intensity levels follow similar trends with $\beta = -10°$ having, the nearest to the wing surface, shear layer.

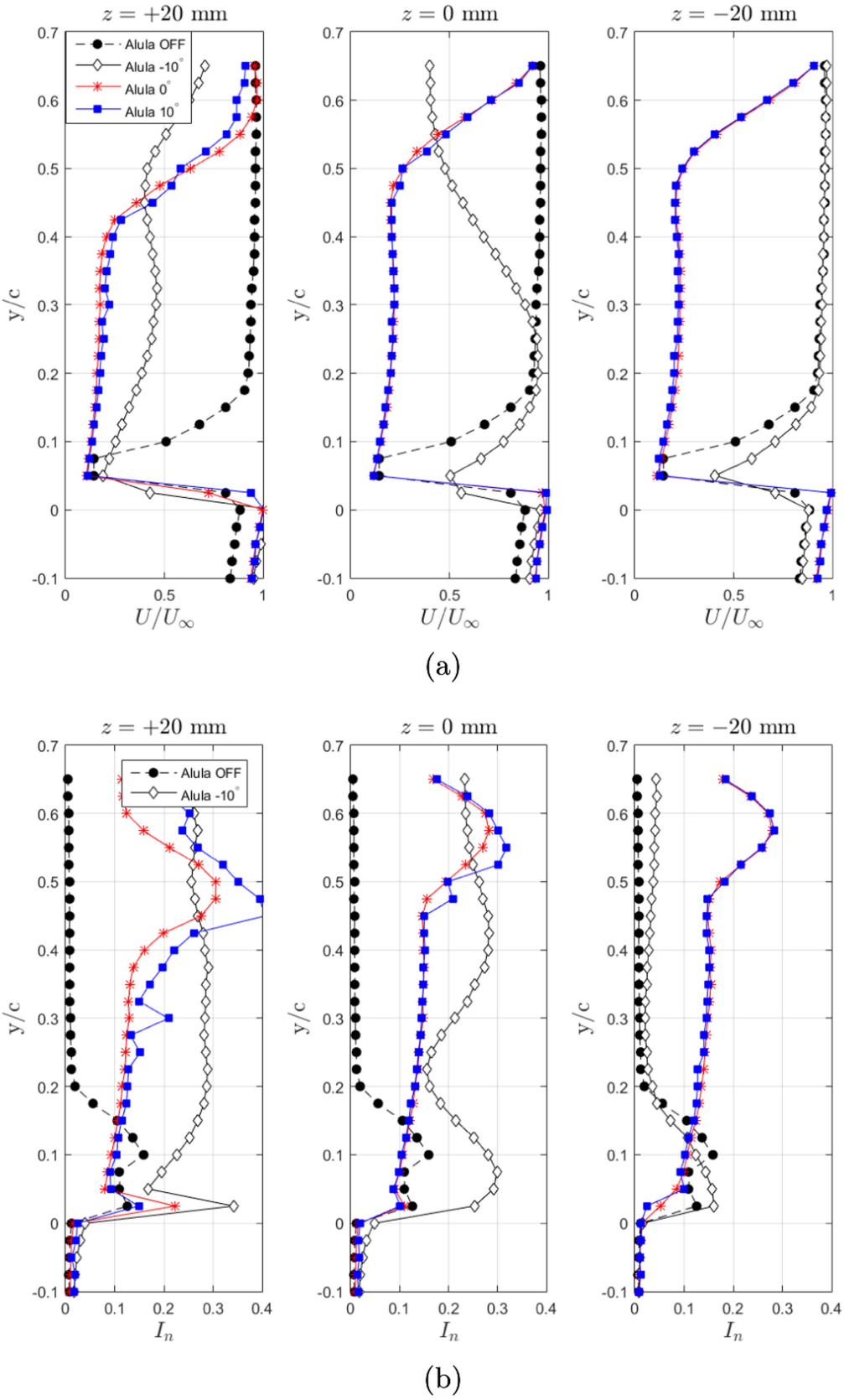

Figure 15. (a) Wake velocity profiles, U/U_∞ and (b) turbulence intensity levels, I_n for the airfoil with and without an alula-inspired device at $\alpha = 18°$, and $Re = 1.35 \times 10^5$. The alula effect is primarily seen at the inboard section of the alula, $z = +20$ mm, with $\beta = -10°$ reducing the velocity deficit the most. Turbulence intensity levels follow similar trends with $\beta = -10°$ having, the nearest to the wing surface, shear layer.

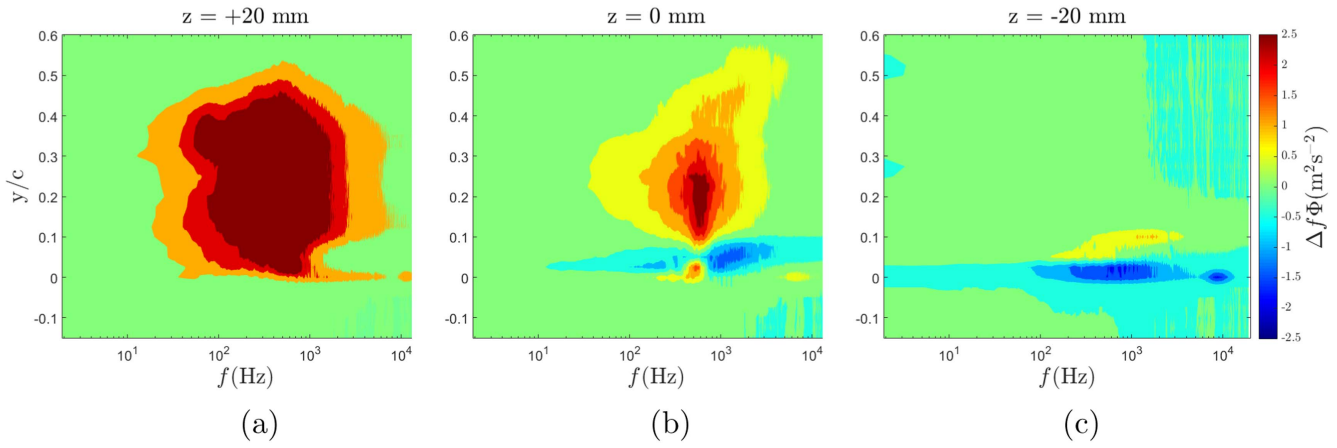

Figure 16. Premultiplied spectral difference of the velocity fluctuations at $Re = 1.35 \times 10^5$, $\alpha = 10°$, and $\beta = -10°$.

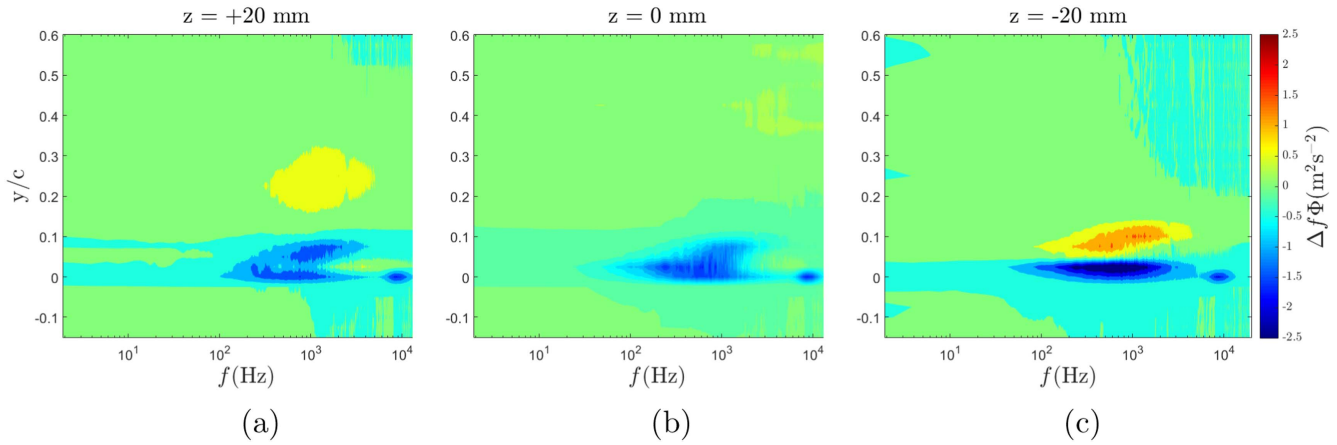

Figure 17. Premultiplied spectral difference of the velocity fluctuations at $Re = 1.35 \times 10^5$, $\alpha = 10°$, and $\beta = 0°$.

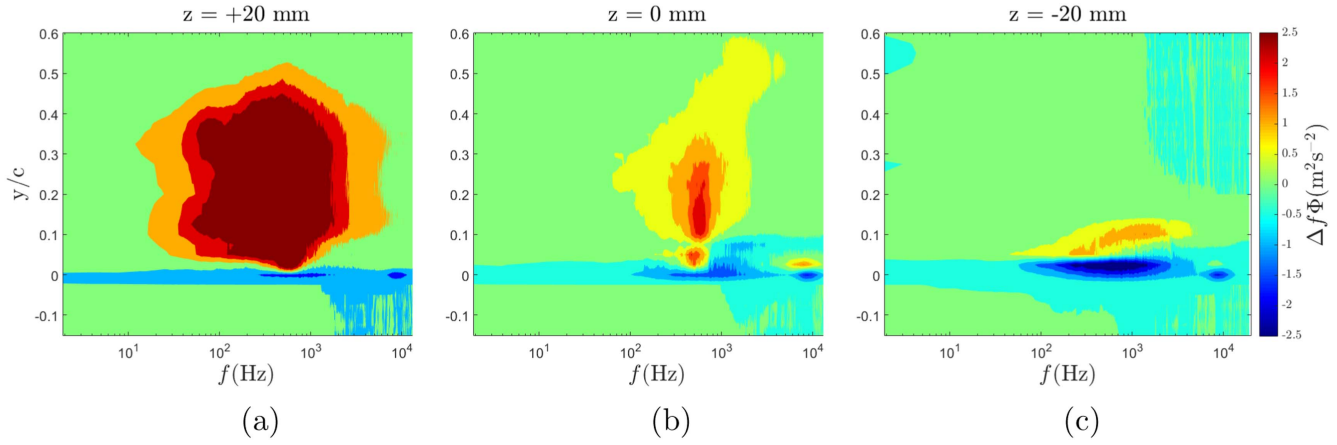

Figure 18. Premultiplied spectral difference of the velocity fluctuations at $Re = 1.35 \times 10^5$, $\alpha = 10°$, and $\beta = 10°$.

velocity recovery of the BL for all span locations (figure 12(a)). As expected at higher wing AoA, lower alula angles perform better since the local flow conditions allow for attached flow. The overlapping velocity profiles for the baseline case, $\beta = 0°$, and $10°$ indicate that the alula is stalled and therefore unable to modify the wake size and move the shear layer closer to the wing surface. The results confirm the observations made from the interactions between β and γ on figure 10(c), i.e. at $\gamma = 13°$, the lower alula angles produce the highest improvements in C_l.

4.2. Lift and wake profile for Re = 1.35 × 10⁵

At $Re = 1.35 \times 10^5$, stall is observed at $\alpha = 13°$ for the S1223 airfoil. Hence at $\alpha = 4°$, the trend is similar to $Re = 1.0 \times 10^5$, the BL is attached and the LEAD has a mostly

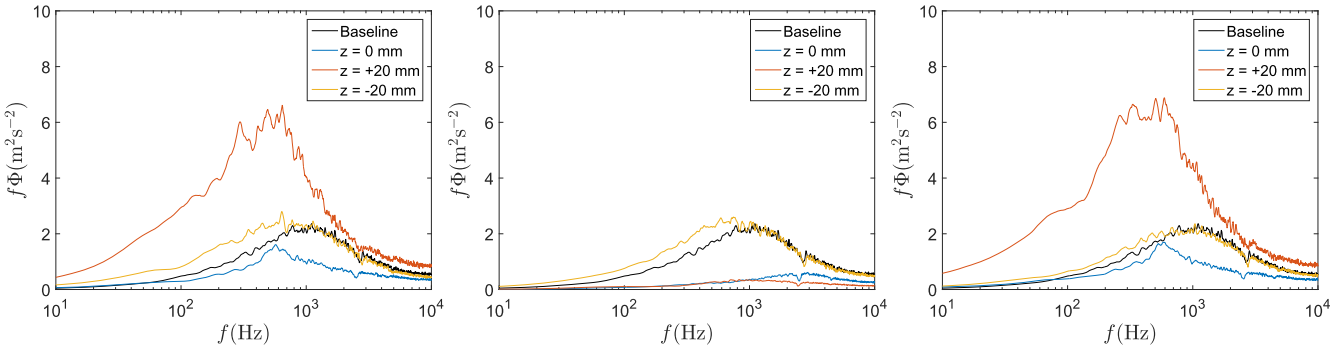

Figure 19. Pre-multiplied spectra ($f\Phi$) comparison at three alula configurations. As evidenced by the spectral difference, at $z = +20, -20$ mm there is a shift in the most energetic structures towards larger scales with higher energy. $Re = 1.35 \times 10^5$, $\alpha = 10°$.

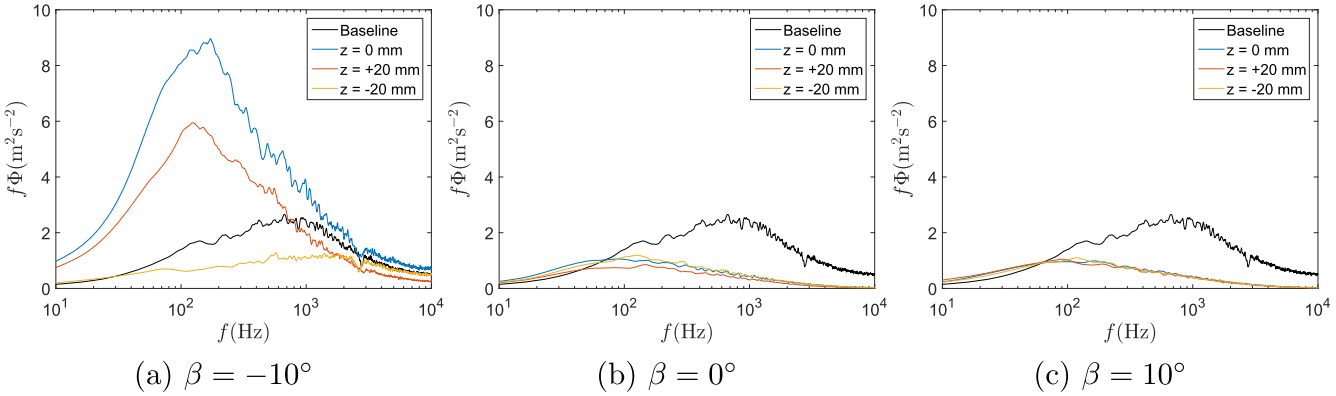

Figure 20. Pre-multiplied spectra($f\Phi$) comparison at three alula configurations. As evidenced by the spectral difference, at $z = -20$ mm there is a shift in the most energetic structures towards smaller scales with lower energy. This shift is linked with delay in flow reversal and reduced wake size. $Re = 1.35 \times 10^5$, $\alpha = 18°$.

negative impact on lift production (figure 13). With the exception of a slight improvement in C_l at $\alpha = 4°$ and $\beta = -5°$ and 0°, the alula remains a poor choice for wing angles below that of the onset of stall. Figure 13(b) shows the effect of the alula morphological parameters on the lift coefficient at $\alpha = 10°$. The effect of the alula is, again, adverse with slight improvements at $\beta > -5°$ and $\gamma = 13°$. At a wing AoA of $\alpha = 18°$, figure 13(c) show that C_l improvements are observed at all alula configurations tested, which is indicative of the positive impact the alula has on the post stall flow conditions.

At AoA $\alpha = 10°$, the velocity profiles (figure 14(a)) provide an explanation of the reduction in C_l due the presence of the alula. Inboard of the alula tip, the wake velocity deficit is increased at both $\beta = -10°$ and 10°. Similar to $Re = 1.0 \times 10^5$, only $\beta = 0°$ shows minimal wake deficit improvements at $y/c - 0.25$ with no impact on the velocity profile at the alula tip and outboard span locations. Turbulence intensity plots (figure 14(b)) shows that the alula configurations at $\beta = -10°$ and 10°, extend the wake shear layer of the wing far beyond $y/c = 0.2$ (baseline).

The wake velocity deficit at $\alpha = 18°$ and $\beta = -10°$ is reduced the most, similar to $Re = 1.0 \times 10^5$ in that at. However, at $Re = 1.35 \times 10^5$, the wake deficit appears to be negatively affected at the alula inboard section, suggesting the suppression of the alula slat effect. At this span location, the flow velocity is slowed to a third of the freestream value, and the turbulence intensity levels are close to 30%, the highest among all alula configurations. At the alula tip location and at $\beta = -10°$, much of the wake deficit is recovered in the near surface BL, which suggests delayed flow reversal. Moreover at 20 mm outboard of the alula tip ($z = -20$ mm), the wing surface BL continues to improve over baseline conditions.

Variation in C_l results observed at $\beta = 5°$, and $\beta = -5°$ and at $\gamma = 4°$, figures 10 and 13, cannot be attributed to the data acquisition system due to the low aggregate error and minimal uncertainty (see section 3). Rather, an explanation may be found in the transient behavior of a laminar separation bubble when changing the AoA. The S1223 is characterized by low-*Re* hysteresis in C_l when crossing the stall region while reducing the wing AoA. To minimize the effect of this behavior all tests are conducted with the wing AoA increasing from zero lift AoA ($\sim -7°$) to the desired test AoA. Even though 10 seconds of rest is provided before data recording was initiated, at low *Re* this time interval may not have been long enough for an expanding or contracting laminar separation bubble to settle. This could result in large deviations of the measured force quantities as observed in the force coefficient results presented in figures 10 and 13.

4.3. Flow structure

Spectral decomposition of the flow was performed in order to infer the prevalent energy structures in the wake of the airfoil at various *Re*, AoA, and alula configurations. The differences in the turbulence energy cascade with the addition of an alula device are analyzed through the spectral differences ($\Delta(f\Phi) = f\Phi_{\text{alula}} - f\Phi_{\text{noalula}}$) of several test configurations and are shown in figures 16–18.

The wake deficit and turbulence intensity for $Re = 1.35 \times 10^5$ and $\alpha = 10^\circ$ and the spectral difference shown in figures 16–18 confirm the hypothesis that at $\beta = 0^\circ$, the alula is operating in favorable local flow conditions. Figure 17(a) shows roughly no increase of turbulence scales compared to $\beta = -10^\circ$ (figure 16(a)) and $\beta = 10^\circ$ (figure 18(a)). This trend is also observed at the alula tip ($z = 0$ mm) span-wise location. At the outboard spanwise location ($z = -20$ mm), there is no observable difference between the wake profiles between alula configurations, which may be attributed to the weak circulation created by the alula. Furthermore, without a strong alula bound circulation, the influence zone from the tip vortex is smaller. The combination of lower flow velocity and adverse pressure gradient over an airfoil at high AoA might explain the premature vortex breakdown. Thus, if β is inappropriate for the local flow conditions and γ is high, the distance between the alula tip and wing surface may be too large for a weak vortex in a strong adverse pressure gradient to positively affect the surface BL.

To further highlight the changes imposed on the surface BL, $f\Phi$ is compared at each spanwise wing location for $\alpha = 10^\circ$ and $Re = 1.35 \times 10^5$ (figure 19). The velocity spectra are taken at a location above the wing surface, at $y/c = 0.075$, close to the center of the developed BL. The inboard of the alula tip location, $z = +20$ mm, exhibits the largest addition of turbulence energy into the wake of the airfoil (figures 16–18). Figures 19(a) and (c) show that alula configurations, which produce higher velocity deficits, $\beta = -10^\circ$ and $\beta = 10^\circ$, there is a shift on the power spectra towards lower frequencies. Thus, the alula has the ability to modulate the size of the shed eddies and their energy levels, which can provide an explanation for the high BL average velocity levels.

At deep stall AoA, $\alpha = 18^\circ$,the velocity deficit is significantly reduced when compared against the baseline configuration at the outboard sections, $z = 0$ mm, $z = -20$ mm, and $\beta = -10^\circ$ (figure 15). A shift towards the left of the frequency domain, i.e. towards higher energy scales, is observed at $z = +20$ mm and $z = 0$ mm (figure 20), while at $z = -20$ mm, the outboard-most location, the turbulence energy is reduced and shifted to the right. From the presented power spectra it becomes clear that only in conditions where the alula shifts the power spectrum towards smaller, lower energy scales, the wake size is reduced. This is not a necessary condition for delaying the flow separation from the wing. Thus, in favorable conditions, with the introduction of a LEAD can re-energize the surface BL to sustain longer runs of attached flow and delay separation.

5. Conclusion

The force and hot-wire wake profile results presented provide an insight into the way an alula-inspired LE device can affect the flow conditions around an airfoil. The critical flow parameters are Reynolds number and main wing incidence angle at pre-stall and post stall conditions. During the experiments two geometric parameters were varied namely, the alula deflection angle and alula relative angle of attack. These parameters were set to the following values: $\beta = -10^\circ, -5^\circ, 0^\circ, 5^\circ, 10^\circ$ and $\gamma = 4^\circ, 13^\circ, 22^\circ$. Force data and hot-wire wake velocity profile analysis indicate that:

(i) In the pre-stall region for both *Re* regimes, the alula shows an adverse effect on the flow structures over the airfoil and negatively impacts C_l values.
(ii) In the post-stall range, a positive impact from the LEAD on the near wall BL is observed at lower alula angles of attack. Alula configuration with the lower relative anglse of attack tend to improve lift the most at post-stall angles of attack.
(iii) A consistent trend in γ is observed for all tested α and *Re* more specifically, an increase from $\gamma = 4^\circ$ to 22° has a positive impact on measured C_l.
(iv) The wake velocity deficit and turbulence intensity plots confirm the measured C_l trends for a given alula configuration, i.e. configurations that have lower turbulence levels and reduced wake deficit, generated higher values of lift.
(v) Pre-multiplied spectral difference ($\Delta(f\Phi)$) between baseline and alula configurations indicate that by modulating the energy levels that exists in the flow structures, particularly in the near surface BL, the average flow velocities can be increased significantly. An increase in the average flow velocity may be related to delayed separation.

The aforementioned effects of the deployed alula device on the flow conditions agree with published results of experiments performed on birds [18].

6. Future work

The results from these experiments show the potential for an alula-inspired LE device to enhance lift production through separation control and stall mitigation. However, the flow field over an airfoil in the presence of a LE device is complicated and requires access to the full flow field to draw a complete picture of the aerodynamic mechanisms. Future work will include capturing the full flow field using PIV. This will not only yield a dense vector field over the entire sample region, but will also provide a way to visualize the complex flow patterns.

In an effort to isolate the effect of an alula-inspired LE device on the near wall BL dynamics, a two-dimensional test configuration was selected for this study. Future plans include extending the experimental work to a three-dimensional

configuration. Using the three-dimensional experimental data, we will test the hypothesis that alula produces tip vortices that create a spanwise flow barrier that arrests the propagation of reversed flow to the outer regions of the wing. This barrier enables birds to continue to produce lift and maintain control authority during high AoA maneuvers.

Acknowledgments

The authors acknowledge support from the Mechanical Science and Engineering Department at the University of Illinois Urbana-Champaign. Resources from the Renewable Energy and Turbulent Environment group as well as the Bio-inspired Adaptive Morphology Lab are greatly appreciated.

References

[1] Videler J J 2006 *Avian Flight* (Oxford: Oxford University Press)
[2] Anderson J D Jr 1985 *Fundamentals of Aerodynamics* (New York: McGraw-Hill)
[3] Prandtl L 1928 Motion of fluids with very little viscosity (Washington, DC)
[4] Smith A O 1975 High-lift aerodynamics *J. Aircr.* **12** 501–30
[5] Abbott I H and Von Doenhoff A E 1959 *Theory of Wing Sections, Including a Summary of Airfoil Data* (Chicago: University of Chicago Press)
[6] Weick F E and Platt R C 1933 Wind-tunnel tests on model wing with fowler flap and specially developed leading-edge slot (Langely Field, VA)
[7] Weick F E and Bamber M J 1933 Wind-tunnel tests of a clark y wing with a narrow auxiliary airfoil in different positions (Langely Field, VA)
[8] Weick F E and Sanders R 1934 Wind-tunnel tests on combinations of a wing with fixed auxiliary airfoils having various chords and profiles (Langely Field, VA)
[9] Lee S-i, Kim J, Park H, Jablonski P and Choi H 2015 The function of the alula in avian flight *Sci. Rep.* **5** 9914
[10] Genc M, Lock G and Kaynak U 2008 An experimental and computational study of low re number transitional flows over an aerofoil with leading edge slat *The 26th Congress of ICAS and 8th AIAA ATIO* p 8877
[11] Shyy W, Aono H, Chimakurthi S K, Trizila P, Kang C-K, Cesnik C E and Liu H 2010 Recent progress in flapping wing aerodynamics and aeroelasticity *Prog. Aerosp. Sci.* **46** 284–327
[12] Whitford R 1991 Four decades of transonic fighter design *J. Aircr.* **28** 805–11
[13] Yao C, Lin J and Allen B 2002 Flowfield measurement of device-induced embedded streamwise vortex on a flat plate *1st Flow Control Conf.* p 3162
[14] Shim H and Park S-O 2015 Passive control of pitch-break of a bwb ucav model using vortex generator *J. Mech. Sci. Technol.* **29** 1103
[15] Cranston B, Laux C and Altman A 2012 Leading edge serrations on flat plates at low reynolds number *50th AIAA Aerospace Sciences Meeting including the New Horizons Forum and Aerospace Exposition* p 53
[16] Shan H, Jiang L, Liu C, Love M and Maines B 2008 Numerical study of passive and active flow separation control over a naca0012 airfoil *Comput. Fluids* **37** 975–92
[17] Meseguer J, Franchini S, Pérez-Grande I and Sanz J 2005 On the aerodynamics of leading-edge high-lift devices of avian wings *Proc. Inst. Mech. Eng.* G **219** 63–8
[18] Austin B and Anderson A M 2007 The alula and its aerodynamic effect on avian flight *ASME 2007 Int. Mechanical Engineering Congress and Exposition* (American Society of Mechanical Engineers) pp 797–806
[19] Khan M A, Dwivedi Y, Khan M, Kiran M and James K K 2013 Comparative aerodynamic study of effect of alula on two birds pigeon & parrot wings *Int. J. Eng. Res. Technol.* **2** 9
[20] Alvarez J, Meseguer J, Meseguer E and Pérez A 2001 On the role of the alula in the steady flight of birds *Ardeola* **48** 161–73
[21] Greenewalt C H 1975 The flight of birds: the significant dimensions, their departure from the requirements for dimensional similarity, and the effect on flight aerodynamics of that departure *Trans. Am. Phil. Soc.* **65** 1–67
[22] Savile D 1957 Adaptive evolution in the avian wing *Evolution* **11** 212–24
[23] Norberg U M 2012 *Vertebrate flight: Mechanics, Physiology, Morphology, Ecology and Evolution* vol 27 (Berlin: Springer)
[24] Nachtigall P D W and Wieser J 1966 Profilmessungen am taubenflügel *Z. Vergleichende Physiol.* **52** 333–46
[25] Kline S and McClintock F 1953 Describing uncertainties in single sample experiments *Mech. Eng.* **75** 3–8
[26] Barlow J, Rae W and Pope A 1999 *Low-Speed Wind Tunnel Testing* (New York: Wiley)
[27] Norberg U M 1979 Morphology of the wings, legs and tail of three coniferous forest tits, the goldcrest, and the treecreeper in relation to locomotor pattern and feeding station selection *Phil. Trans. R. Soc.* B **287** 131–65
[28] Norberg U M 1994 Wing design, flight performance, and habitat use in bats *Ecological Morphology: Integrative Organismal Biology* ed P C Wainwright and S M Reilly (Chicago: University of Chicago Press) pp 205–39
[29] Liu T, Kuykendoll K, Rhew R and Jones S 2006 Avian wing geometry and kinematics *AIAA J.* **44** 954–63
[30] Carruthers A, Walker S, Thomas A and Taylor G 2010 Aerodynamics of aerofoil sections measured on a free-flying bird *Proc. Inst. Mech. Eng.* G **224** 855–64
[31] Gopalarathnam A and Selig M S 2001 Low-speed natural-laminar-flow airfoils: case study in inverse airfoil design *J. Aircr.* **38** 57–63
[32] Selig M S 1995 *Summary of Low Speed Airfoil Data* vol 1 (SoarTech)